Double-integrating-sphere system for measuring the optical properties of tissue

John W. Pickering, Scott A. Prahl, Niek van Wieringen, Johan F. Beek, Henricus J. C. M. Sterenborg, and Martin J. C. van Gemert

A system is described and evaluated for the simultaneous measurement of the intrinsic optical properties of tissue: the scattering coefficient, the absorption coefficient, and the anisotropy factor. This system synthesizes the theory of two integrating spheres and an intervening scattering sample with the inverse adding–doubling algorithm, which employs the adding–doubling solution of the radiative transfer equation to determine the optical properties from the measurement of the light flux within each sphere and of the unscattered transmission. The optical properties may be determined simultaneously, which allows for measurements to be made while the sample undergoes heating, chemical change, or some other external stimulus. An experimental validation of the system with tissue phantoms resulted in the determination of the optical properties with a $<5\%$ deviation when the optical density was between 1 and 10 and the albedo was between 0.4 and 0.95.

Key words: Optical properties, absorption coefficient, scattering coefficient, anisotropy factor, integrating sphere, adding–doubling, tissue optics.

1. Introduction

With progress in laser medicine there is an ever-increasing need to provide accurate measurements of the optical properties of biological tissues. The purpose of this paper is to present a synthesis of what we believe is the most appropriate solution to the radiative transfer equation[1] with a measuring technique that allows the accurate and simultaneous determination of the (*in vitro*) absorption and scattering coefficients and the anisotropy of scattering.

Cheong *et al.*[2] provided a list of optical properties measured by a variety of techniques. These techniques and their associated advantages and disadvantages were also discussed. The extreme variation in the properties of some tissues measured by different techniques (assuming that no gross errors were made) may be attributed to differences between *in vivo* and *in vitro* measurements, differences in radiative transfer models, differences in tissue preparation, or differences in measuring techniques (with the possibility of systematic errors).

Light propagation in turbid media is characterized by the absorption coefficient μ_a, the scattering coefficient μ_s, the scattering phase function, the refractive index, and the surface conditions (rough or smooth).

The measurement of refractive indices and surface conditions is important when light distributions near boundaries are considered, and measuring techniques that are radically different from those discussed here are required; thus we shall not consider them further.[3]

The direct phase-function measurements performed by goniometry on thin slices of tissue have established the preference for the Henyey–Greenstein phase function, which describes the forward-scattering nature of most tissues.[4–7] This phase function may be described by the average cosine of the scattering angle, the anisotropy factor g, where $g = 0$ denotes isotropic scattering and $g = 1$ is totally forward scattering. The method used in this paper enables the calculation of the anisotropy under the assumption of the Henyey–Greenstein phase function.

In vivo measurements are the most immediately applicable to dosimetry; yet they present techniques that provide only limited information on optical properties. Interstitial fiber techniques (invasive) give the effective attenuation coefficient μ_{eff} and

When this research was done the authors were with the Laser Centre, Academic Medical Centre, Meibergdreef 9, 1105 AZ, Amsterdam, The Netherlands. S. A. Prahl is now with Wellman Laboratories of Photomedicine, Massachusetts General Hospital, Boston, Massachusetts 02114.

Received 12 November 1991.
0003-6935/93/040399-12$05.00/0.

sometimes the absorption μ_a and reduced scattering coefficient $[\mu_s' = \mu_s(1 - g)]$.[8–10] Reflectance and transmittance measurements as a function of source and detector position allow similarly the determination of μ_a and μ_s'.[11,12] Several new techniques are under development that also yield optical properties; in particular, photoacoustic spectroscopy[13,14] yields μ_a, and time-of-flight measurements[15,16] and pulsed photothermal radiometry[17,18] yield μ_s' and μ_a.

In vitro measurements have the advantage over *in vivo* measurements in that the effect of individual tissue structures (for example, the epidermis and the dermis instead of the entire skin) may be evaluated. However, they are also subject to preparation artifacts. Other than the goniometric measurements the majority of techniques involve the use of integrating spheres to measure reflection and transmission.

The theory and practicality of integrating spheres for measuring the reflectance of a sample have been studied extensively.[19–23] Much of this knowledge is still applicable to transmission measurements.[24] The measurements of the reflection, the total transmission, and the sample thickness allow the determination of μ_a and μ_s'. The additional measurement of the collimated transmission allows the separation of the reduced scattering coefficient into the scattering coefficient and the anisotropy. This measurement has been made often with a separate, thinner, sample because of the difficulties in detecting small quantities of light. However, if the measurements of reflection and diffuse and collimated transmission are all made from one sample placed between two integrating spheres, as described in this paper, all three optical properties may be deduced simultaneously. Our principal reason for developing this system for the simultaneous determination of optical properties is that it allows the investigation of the changes in optical properties during the application of heat. Furthermore, such a system requires only the minimal preparation of one tissue sample. We shall describe the practicalities of this system including the methodology of determining the influence of the sphere parameters, taking into account the exchange of light between the spheres,[25] avoiding light losses from the sample, the overall accuracy to which optical properties can be determined, and the importance of an accurate collimated transmission measurement. In addition, if collimated transmission measurements are impractical (for example, with optically thick samples), we show that it is more accurate to use collimated incident light as opposed to diffuse incident light for reflection and total transmission measurements.

To determine the optical properties from the measured light flux in the two spheres and the collimated transmitted light flux, we use an iterative method with the adding–doubling solution of the radiative transfer equation. This inverse adding–doubling algorithm is discussed in a sister paper.[1] Briefly we chose this solution because it allows the use of collimated and diffuse incident light, is applicable with slab geometry, can account for boundary conditions, and is relatively fast in computation. Please note that, because our goal is to obtain the absorption and scattering characteristics of the tissue, we do not attempt to calculate the percentage of light reflected or transmitted by the sample, but rather we calculate the expected flux in each sphere with the adding–doubling algorithm and by using the sphere formulas described in Section 2. We compare this with the measured fluxes. When they do not match, a new set of optical properties is used to recalculate the fluxes, and these are once more compared with the measured fluxes. This iterative process continues until the experimental and calculated fluxes match, giving the optical properties of the sample.

2. Integrating-Sphere Theory

Although the integrating-sphere theory has been studied extensively, we introduce the formulas applicable for the single integrating sphere and discuss how they extend to double integrating spheres. (The mathematical part of this theory has been described in another paper.[25]) Sphere formulas for both diffuse incident and collimated incident light are given since they are necessary for understanding the procedures for calibrating the spheres (Section 3).

A. Single-Sphere Theory

To measure the reflected and transmitted light from a sample, we situated it at, respectively, the exit or entrance port of a sphere. Normally the detector is situated on the inner sphere surface. Often tissue is placed between glass plates to prevent dehydration, to provide mechanical support, and to minimize surface effects. The influence of these plates on the reflected and transmitted light may be calculated.[1] However, the theory requires that no directly reflected light (Fresnel reflected) from the sample irradiates the detector; therefore a baffle is placed between the sample and the detector (Fig. 1).

The integrating-sphere theory accounts for the losses caused by absorption from the sphere wall and light escaping the sphere. The power detected depends on the total light remaining within the sphere and on the relative (to the total sphere area) size of the detector.[18–25]

For a single-sphere reflectance measurement using diffuse irradiance of the sample [generated by the light entering the sphere irradiating the sphere wall; Fig. 1(a)], the power detected on the inner surface of the sphere is

$$P_d = \frac{b_1\left(1 - R_d \frac{A_s}{A}\right)}{1 - b_2 R_d} P, \tag{1}$$

where P is the power of the incident light, R_d is the diffuse reflectance of the sample for diffuse irradiance, A_s is the sample area, A is the inner surface area of the complete sphere, and the sphere constants b_1

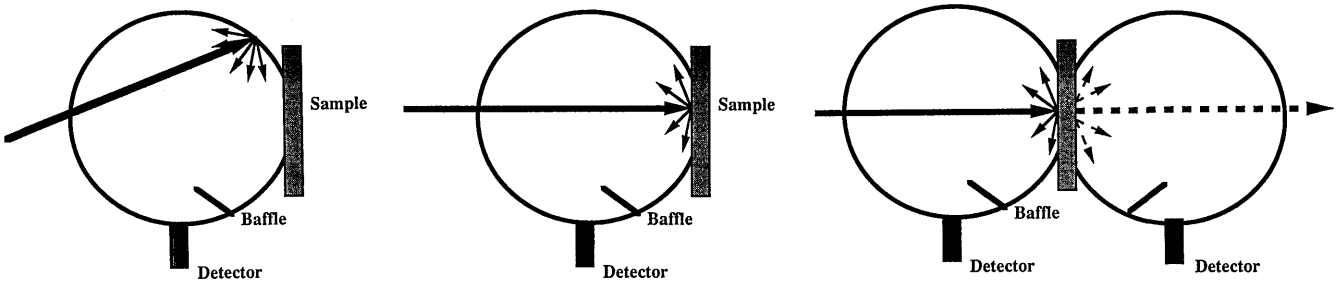

(a) (b) (c)

Fig. 1. (a) Diffuse light may irradiate the sample through the beam first irradiating the sidewall of the sphere. (b) Alternatively collimated light may directly irradiate the sample. In all cases a baffle is placed between the sample and the detector to prevent detection of specularly reflected light. In the double-sphere system the sample is placed between the spheres, and the unscattered collimated transmitted light is permitted to leave the system (c).

and b_2 are defined as

$$b_1 = \frac{A_\delta}{A}\frac{m}{1-m\alpha}, \qquad b_2 = \frac{A_s}{A}\frac{1}{1-m\alpha}, \tag{2}$$

where m is the diffuse reflectance factor of the sphere wall, A_δ is the area of the detector, α is the fraction of the total sphere area occupied by the sphere wall,

$$\alpha = [A - (A_s + A_\delta + A_a)]/A. \tag{3}$$

(A_a is the sum of the area of all other apertures in the sphere wall.) The term $(1 - R_d A_s/A)$ accounts for the presence of a baffle between the detector and sample [see Eq. (4b) in Ref. 25]. For the spheres discussed in this paper this results in at most a 3% correction, which, compared with other sources of uncertainty, is small (see Sections 4 and 5) and therefore for the sake of clarity is not included in the rest of this paper.

For collimated light that is first incident on the sample [Fig. 1(b)] the detected power is

$$P_d = \frac{b_1(\alpha R_{cd} + R_c)}{1 - b_2 R_d} P, \tag{4}$$

where R_{cd} is the diffuse reflectance of the sample for collimated irradiance and R_c is the specular (unscattered) Fresnel reflection of the sample for collimated irradiance. (Note that if this light is permitted to pass out of the sphere, this term is zero.)

For a sample located at the entrance port of a sphere and for diffuse irradiance, the detected power is

$$P_d = \frac{b_1 \alpha T_d}{1 - b_2 R_d} P, \tag{5}$$

where T_d is the coefficient of transmittance for diffuse irradiance. For collimated irradiance the detected power is

$$P_d = \frac{b_1(T_c + \alpha T_{cd})}{1 - b_2 R_d} P, \tag{6}$$

where T_{cd} is the diffuse transmittance for collimated irradiance and T_c is the collimated (unscattered) transmittance for collimated irradiance. (Note that if the collimated light is permitted to pass out of the sphere, this term is zero.)

If a nonisotropic detector is used as an alternative to a baffle (i.e., a detector such as a fiber optic that detects only light that is coming from part of the sphere wall, a part not containing the sample), the equations are identical with the exception of b_1, which is smaller by a factor depending on the fraction of the sphere wall from where the detector receives light.[25]

B. Double-Sphere Theory

The double-sphere system consists of two spheres with the sample placed between them [Fig. 1(c)]. The two spheres may be of different geometries and with different surface reflectances. The only requirement are that the sample ports be the same area A_s and shape and that the reflectance and transmittance factors of the sample be independent of the side of the sample at which the light is incident. If light irradiates the sample in the first sphere (called the reflectance sphere), a portion of this light will be transmitted through the sample to the second sphere (the transmittance sphere). Some of the light within the transmittance sphere will irradiate the sample (the back of the sample), and some of this light will be transmitted back into the reflectance sphere; thus the signal in the reflectance sphere is increased. Some of this additional light is then (re)transmitted to the transmittance sphere, and the signal in the transmittance sphere is increased. This process of the transmission of an ever-decreasing portion of the light back and forth through the sample continues until all the light has been absorbed or lost from the spheres. The net effect is to increase the signal in both spheres over the single-sphere case. In the following equations the nomenclature is identical to that of the single-sphere equations with the addition of an extra subscript, r or t, to identify the parameters associated with either the reflectance or transmittance spheres, respectively.

For diffuse light incident on the sample in the reflectance sphere (generated by collimated light that is first incident on the sphere wall), the power collected in the reflectance sphere is

$$P_d = \frac{b_{1r}(1 - b_{2t}R_d)}{(1 - b_{2r}R_d)(1 - b_{2t}R_d) - b_{2r}b_{2t}T_d^2} P, \quad (7)$$

and the power detected in the transmittance sphere is

$$P_d = \frac{b_{1t}b_{2r}m_r\alpha_t T_d}{(1 - b_{2r}R_d)(1 - b_{2t}R_d) - b_{2r}b_{2t}T_d^2} P. \quad (8)$$

For collimated light incident on the sample within the reflectance sphere the power detected in the reflectance sphere is

$$P_d = \frac{b_{1r}[(R_c + \alpha_r R_{cd})(1 - b_{2t}R_d) + \alpha_r b_{2t}T_d(T_{cd} + m_t T_c)]}{(1 - b_{2r}R_d)(1 - b_{2t}R_d) - b_{2r}b_{2t}T_d^2} P, \quad (9)$$

and the power detected in the transmittance sphere is

$$P_d = \frac{b_{1t}[(T_c + \alpha_t T_{cd})(1 - b_{2r}R_d) + \alpha_t b_{2r}T_d(R_{cd} + m_r R_c)]}{(1 - b_{2r}R_d)(1 - b_{2t}R_d) - b_{2r}b_{2t}T_d^2} P. \quad (10)$$

These equations, as for the single-sphere equations, account for the losses within the spheres through absorption by the wall and losses through the apertures. However, because of the exchange of light between the spheres each equation must account for light losses within both spheres. These losses will also depend on the amount of light transmitted through the sample; thus the power within the reflectance sphere not only depends on the coefficients of reflectance but also on the coefficients of transmittance. This coupling of the reflection and transmission coefficients implies that they cannot be determined analytically from the measurement of the sphere powers for either of the incident light geometries (diffuse or collimated).

3. Measurement Techniques and Sphere Constants

A. Making Relative Measurements

The voltage recorded by the detector (usually a photodiode or a photomultiplier tube) on the inner surface of each of the spheres is proportional to the total power incident on the detector P_d so that

$$V = KP_d, \quad (11)$$

where K depends on the characteristics of the detector. In practice there is a background signal or voltage V_0 depending on the noise in the detection system and on the presence of stray light. Therefore we may rearrange Eq. (11) to be

$$P_d = \frac{1}{K}(V - V_0). \quad (12)$$

Finding the reflection and transmission coefficients of the sample from measurements of the voltage knolwedge of the sphere constants (b_1, b_2, α, A, s, and m), the initial power, and the detector constant K. Furthermore, there are as many as six unknown coefficients [R_c, R_d, R_cd, T_c, T_d, T_cd; see Eqs. (9) and (10)]. The measurement of the collimated transmittance with a third detector at a distance from the second sphere yields T_c:

$$T_c = \frac{V_c - V_{c,0}}{V_{c,\mathrm{ref}} - V_{c,\mathrm{ref0}}} = V_{c\%}, \quad (13)$$

where V_c is the voltage recorded with the sample in place between the spheres and $V_{c,\mathrm{ref}}$ is the voltage recorded without the sample in place. $V_{c,0} = V_{c,\mathrm{ref0}}$ is the background signal with the light source extinguished. Note that the factor K is eliminated from this equation.

The specular reflection coefficient R_c may be calculated from Fresnel's equations. This leaves at most the diffuse reflection of collimated irradiance R_{cd}, the diffuse reflection of diffuse irradiance R_d, the diffuse transmission of collimated irradiance T_{cd}, and the diffuse transmission of diffuse irradiance T_d to be determined from the voltages measured within the two spheres. The diffuse reflection (or transmission) coefficient of the collimated irradiance is a special case of the coefficient for diffuse irradiance. (Only one incident direction is considered.) Some radiative transfer models, such as adding–doubling, are able to couple the two coefficients because the model is able to consider the direction of the incident light. Therefore there remain only two unknowns (because of the tissue) requiring only the measurement of the voltages in the two spheres. The other unknowns, P, K, and the sphere constants, may be measured or eliminated through the procedures described below.

The power P of the incident beam can be measured directly, but for convenience we took measurements that are relative to the power that we detected by using a standard reference plate (which is diffusely reflecting with reflection coefficient R_{ref}) in the position of the reflecting sample. Therefore for this reference plate the power incident on the detector is

$$P_{d,\text{ref}} = P\phi(R_{\text{ref}}, A_s, A, A_a, m), \tag{14}$$

where the function ϕ is constant for a given sphere geometry and reference plates. Furthermore this function depends on whether collimated or diffuse light is incident on the reference plate.

By combining Eq. (12) and (14), we may write

$$P = \frac{P_{d,\text{ref}}}{\phi} = \frac{\frac{1}{K}(V_{\text{ref}} - V_{\text{ref},0})}{\phi}, \tag{15}$$

where V_{ref} is the voltage measured with the reference plate in position and $V_{\text{ref},0}$ is the background measurement with no reference plate.

Combining Eqs. (12) and (15) gives the ratio of the detected power to the incident power as

$$\frac{P_d}{P} = \phi \frac{(V - V_0)}{(V_{\text{ref}} - V_{\text{ref},0})} = \phi V_{\%}, \tag{16}$$

which is independent of the constant K.

From the equations for the detected power [Eqs. (1) and (4)–(10)] we note that

$$\frac{P_d}{P} \propto b_1. \tag{17}$$

Therefore we may define b_1 as

$$b_1 \equiv b_1 \frac{1}{\phi}. \tag{18}$$

Thus the need to measure the power is eliminated, and the reflectance of the sample can be obtained from the measurement of the four voltages (V, V_0, V_{ref}, $V_{\text{ref},0}$) and knowledge of the sphere constants. However, it is necessary that all measurements made with the sample and the reference plate be made with the same incident power. This is a requirement of Eq. (18).

We can write Eqs. (1) and (4)–(10) in terms of $V_{\%}$ by utilizing the above definition of b_1 and replacing P_d/P by $V_{\%}$. The measurements required to measure $V_{\%}$ for the reflectance and each of the transmittances are summarized in Table 1. Note that where there is a need to distinguish between the voltages measured within the reflectance sphere and those measured with the transmittance spheres, they have an additional subscript of r and t, respectively. Furthermore all reference voltages in the transmittance sphere must be made in the absence of the reflectance sphere and with the sphere rotated so that the the exit port in the double-sphere geometry becomes the entrance port.

Table 1. Voltage Measurements Required to Determine V%

Measurement	Reflectance and Transmittance Spheres
V, (V_r, V_t)	With the sample
V_0, ($V_{r,0}$, $V_{t,0}$)	Without the sample
V_{ref}, ($V_{r,\text{ref}}$, $V_{t,\text{ref}}$[a])	With the reference plate
$V_{\text{ref}0}$, ($V_{r,\text{ref}0}$, $V_{t,\text{ref}0}$,[a] $V_{t,\text{ref}0'}$)	Without the reference plate, single sphere
Measurement	Collimated transmittance
V_c	With the sample
$V_{c,0} = V_{c,\text{ref}0}$	With the beam blocked

[a]For the transmittance sphere the sphere geometry must be reversed.

B. Determination of Sphere Constants

If all the geometric properties of the sphere are known (wall area A, sample area A_s, and other aperture areas A_a) along with the reflectance of the sphere wall m, b_2 [Eq. (2)] may be calculated. Similarly with these parameters and with A_δ and ϕ, b_1 may be calculated. In practice, however, ϕ is unknown, many of the other parameters may not be known exactly, and the sphere constants need to be measured.

The sphere parameters b_1 and b_2 can be found most easily with diffuse irradiance. Equation (1) now applies with $V_{\%}$ in place of P_d/P, and b_1 is as defined in Eq. (18). If no sample is present,

$$V_{\%} = b_1. \tag{19}$$

With the addition of a diffusely reflecting standard of known reflectance, b_2 can be measured by a rearrangement of Eq. (1) (ignoring the influence of a baffle) to give

$$b_2 = \frac{b_1 - V_{\%}}{V_{\%} R_{ds}}, \tag{20}$$

where R_{ds} is the known diffuse reflectance of a standard.

In the collimated case there is also an α factor within Eq. (4), which may be calculated with Eq. (3) from knowledge of the sphere geometry (i.e., the sphere area, the sample area, and other aperture areas).

When b_1 and b_2 are measured and A_s/A and α are calculated, only the sphere reflectance m remains undetermined. This may be determined by rearranging Eq. (2):

$$m = \frac{-\frac{A_s}{A} + b_2}{\alpha b_2}. \tag{21}$$

Since m is unlikely to change significantly, only occasionally do we check its value (for any slow degradation in the quality of the sphere reflectance). Therefore, as long as the sphere geometry remains unchanged, b_2 remains unchanged. Thus, rather

than measuring b_2 each time, we use a previously determined value and calculate b_1 by a rearrangement of Eq. (4):

$$b_1 = \frac{V_{\%}}{\alpha R_{cds}}(1 - b_2 R_{ds}), \tag{22}$$

where $V_{\%}$ is measured with a standard diffuse reflection plate of known reflectance R_{ds} and collimated incident light. The specularly reflected light R_c is assumed to be lost through the entrance port. Also the diffuse reflectance of collimated incident light of the standard R_{cds} and diffuse reflectance of diffuse incident light R_{ds} are assumed to be identical. (We measured the difference for our standards, the Labsphere SRS-010 series, to be $<1.5\%$.)

With the sphere constants and the measurements that give $V_{r\%}$, $V_{t\%}$, and $V_{c\%}$, we can iterate the albedo a, optical depth τ, and anisotropy g of the sample by using the inverse adding–doubling solution to produce calculated values of $V_{\%}$ within a minimum error to be the same as the measured values.[1] From the albedo, the optical depth, and thickness d of the sample, the scattering and absorption coefficients can be determined:

$$\mu_a = \frac{\tau(1 - a)}{d}, \qquad \mu_s = \frac{a\tau}{d}. \tag{23}$$

4. Theoretical Uncertainties

In this section we discuss the theoretical accuracy to which the reflection and transmission of a sample can be measured. This illustrates that greater accuracy can be obtained when collimated rather than diffuse irradiance is used. Note that to find the optical properties of a sample we do not normally calculate the reflectance and transmittance explicitly as explained in Section 1 and in Ref. 1.

Equation (1) may be rearranged to give the diffuse reflectance

$$R_d = \frac{b_1 - V_{\%}}{b_1 \dfrac{A_s}{A} - b_2 V_{\%}}. \tag{24}$$

To estimate the uncertainty in R_d for an uncertainty in the measured variables ($X_i = b_1$, $V_{\%}$, s, A, b_2), we apply

$$(\Delta R_d)^2 = \sum_i \left(\frac{\partial R_d}{\partial X_i}\Delta X_i\right)^2. \tag{25}$$

Table 2 gives the percentage uncertainty in R_d at $R_d = 0.4$ for 1%, 2%, 5%, and 10% uncertainties in all the other variables. This shows that the uncertainty in reflectance is due primarily to uncertainties in b_1 and in $V_{\%}$. The overall uncertainty is proportional to the measurement uncertainties.

Similarly the diffuse reflectance and its uncertainty can be calculated for collimated incident light. An additional uncertainty is included to account for the assumption that the diffuse reflection of collimated incident light is the same as the diffuse reflection of diffuse incident light. Figure 2 shows the uncertainty in R_d for a 1% uncertainty in all the variables for both diffuse and collimated incident light within a single sphere. Collimated irradiance gives a much more accurate measurement of the reflectance.

We may explain the difference in terms of a signal-to-noise ratio. In the diffuse case there is a signal registered by the detector due to the light within the sphere even when no sample is present. This signal is proportional to b_1. The presence of a diffusely reflecting sample will increase this signal by a factor of $1/(1 - b_2 R_d)$ [Eq. (1)]. Since b_2 is typically ~ 0.25, the maximum factor by which the signal can increase (the 100% reflecting sample) is 1.33. Thus all measurements are made with a high background signal. Noise in this background signal, especially with low-reflectance samples, will result in uncertainties in the calculation of the reflectance. In the collimated case the sample reflectance acts as the source, and there is no independent background signal.

The uncertainty in transmittance depends weakly on the uncertainty in reflectance [Eqs. (5) and (6)] but is approximately just the sum of the uncertainty in the transmittance sphere b_1 and $V_{\%}$.

With the double integrating spheres the uncertainties calculated for the single spheres will also apply. In the reflectance sphere there will be an additional uncertainty caused by the signal returning from the transmittance sphere through the sample. For collimated irradiance this signal is not directly propor-

Table 2. Effect of the Change in Each Variable on the Reflectance for a Given Uncertainty in that Variable at $R_d = 0.41$, $A_s/A = 0.03$, $b_1 = 0.8$, $b_2 = 0.25$ and for Diffuse Incident Light[a]

Uncertainty in X_i (%)	$\Sigma_i\left(\frac{\partial R_d}{\partial X_i}\Delta X_i\right)^2$				$(\Delta R_d)^2$	Uncertainty in R_d (%)
	$X_i = b_1$	$X_i = b_2$	$X_i = A_s/A$	$X_i = V_{\%}$		
1	0.00163	0.00002	0	0.00163	0.00327	14
2	0.00650	0.00008	0	0.00650	0.0131	28
5	0.0406	0.00053	0.000006	0.0406	0.0818	70
10	0.163	0.0021	0.000024	0.163	0.327	140

[a]Using $(\Delta R_d)^2 = \Sigma_i[(\partial R_d/\partial X_i)\Delta X_i]^2$.

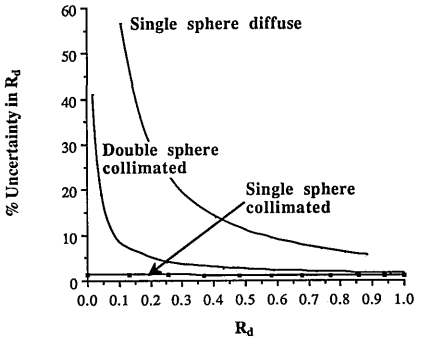

Fig. 2. Uncertainty in the calculated reflectance is always greatest when the reflectance (and hence the signal) is low. For a single sphere diffuse irradiation leads to a much greater uncertainty in the reflectance than collimated irradiation because there is a signal generated prior to the reflection by the sample. With the double-sphere system the uncertainty in reflectance is increased because of the exchange of light between the spheres, but it is still smallest for collimated irradiation, and this uncertainty is smaller than for diffuse irradiation in the single sphere.

tional to the reflectance of the sample (but rather the transmittance) and is maximal when there is no absorption ($R_d = 1 - T_d$). This leads to a greater uncertainty in reflectance than with the single sphere but still much less uncertainty than with diffuse irradiance. (This worst case is included in Fig. 2.)

The preference for collimated irradiance was first discussed by Taylor in 1920.[19] At that time the production of a narrow collimated beam (required for small samples) of sufficient intensity was often not practical. Until recently models of radiative transfer have relied on the assumption of diffuse irradiance. The advent of lasers and radiative transfer models able to cope with collimated irradiance has, in our opinion, rendered the use of diffuse irradiance obsolete given the greater uncertainties involved.

5. Practicalities

While the theory in the sections above will enable the reader to make measurements with the double integrating spheres, there are a number of practical aspects related to the design and method of operation of the equipment that require discussion. Since collimated irradiance gives more accurate measurements, the following sections consider collimated irradiance only.

A. Sample Size

Loss of light through the sides of the sample and sample holder will erroneously increase the calculated absorption coefficient. This loss depends on the physical size and geometry of the sample, the size of the incident beam, and the optical properties of the sample.

As a highly forward scattering and weakly absorbing liquid, Intralipid-10% was used in various dilutions to mimic a range of optical depths of tissue. Previous research has established the optical properties of Intralipid at 633 nm.[10,26,27]

We measured the total light collected for four different combinations of sample port diameters h (10, 19, or 25 mm) and sample thickness d (0.5 or 1.0 mm) with a 1-mm-diameter He–Ne laser (Uniphase 1105).

Light loss was greatest, by as much as 30%, for a small sample port diameter (10 mm) and intermediate optical depths.[2–8] For greater optical depths (at the same port diameter) the lost light is reduced because the scattering is sufficient to prevent a great transport of light to the sample sides. Similarly with a larger port there is reduced light loss. For a 1-mm sample thickness and 25-mm port diameter the light loss was negligible over the optical depth range from 0 to 54.

B. Collimated Detector Distance

The collimated detector measuring unscattered transmitted light $V_{c\%}$ is situated behind the exit port of the transmittance sphere. If this detector is close to the port, it will detect not only unscattered light but also light that has undergone only a few scattering events and possibly some of the diffuse light (as a result of reflections within the sphere) lost through the port. The farther the detector is from the port the less scattered light we detected, depending on the detector size (we used 3-mm-square photodiodes from Telefunken, BPW 34) and the optical depth of the sample.

To find a distance at which virtually all the scattered light has been eliminated from the collimated signal, we measured $V_{c\%}$ with a 5-mW He–Ne laser (Uniphase 1105) as a function of the distance from the sample (Intralipid-10%) and for three different optical depths of the sample ($\tau = 5, 7, 10$). At any given detector distance the higher the optical depth the greater the scattered light contribution to the collimated signal. For optical depths of <10 and any distance exceeding 60 cm, the error in $V_{c\%}$ was $<5\%$.

The collimated transmission measurement determines directly the optical depth of the sample. The inverse adding–doubling program with the measurements within the two spheres will determine the unique albedo and anisotropy.[1] Without the collimated transmission measurement only the reduced albedo and reduced optical depths may be calculated.

C. Sample Holders

A glass (or quartz) sample holder provides mechanical stability and serves to minimize rough surface effects. A drop of water (or some neutral buffered solution) prevents refractive-index mismatches between the sample and glass.

Sometimes with coherent collimated light there is interference from the glass slides. This occurs with two parallel slides when the reflection from the air glass surface and the glass sample surface are such that for certain directions of the incident light constructive or destructive interference may occur (which is similar to a Fabry–Perot interferometer). We found that this interference experimentally has a considerable effect on the signal from the reflected

light. The problem may be overcome by the utilization of slides with nonparallel surfaces or optical flats.

D. Background Measurements

With our technique we measure with a lock-in amplifier and a chopped irradiance. This all but eliminates any background signal from extraneous light sources. Therefore, the measurement of V_0, the background signal, in each of the spheres is made while the light source is on and no sample is present. Occasionally the background signals measured in the double-sphere configuration ($V_{r,0}$ and $V_{t,0}$) can be comparable with the signal when the sample is present; almost invariably this is a result of poor collimation of the beam (such as when nonlaser sources or laser light from a fiber is used). These background signals are directly proportional to the total source power. Furthermore, the background signal for the reference measurements ($V_{r,\mathrm{ref0}}$ and $V_{t,\mathrm{ref0}}$) made in a single-sphere configuration is always lower. We conclude that this noise is due principally to the divergence of the beam, which results in some light hitting the back wall of the transmittance sphere rather than exiting the port through which the collimated signal is measured. However, in the presence of a sample this noise will be reduced because of the absorbance and scattering of the sample. To correct for this noise we must calculate the exchange of light between the spheres for this noise.

If we redefine $V_{\%}$ as

$$V_{\%} = \frac{V - V_{\mathrm{dark}}}{V_{\mathrm{ref}} - V_{\mathrm{dark}}}, \tag{26}$$

where V_{dark} is the signal measured with the light source blocked. $V_{r\%}$ and $V_{t\%}$ may then be corrected by

$$V_{r\%}^{\mathrm{corrected}} = V_{r\%} - F_1 V_{r,\mathrm{ref0}\%} - F_2 V_{t,\mathrm{ref0}'\%}, \tag{27}$$

$$V_{t\%}^{\mathrm{corrected}} = V_{t\%} - F_3 V_{r,\mathrm{ref0}\%} - F_4 V_{t,\mathrm{ref0}'\%}, \tag{28}$$

where all measurements are given relative to the reference plate measurement [Eq. (26)], $V_{r,\mathrm{ref0}\%}$ is measured with the reflectance sphere in position without the transmittance sphere, and $V_{t,\mathrm{ref0}'\%}$ is measured with the transmittance sphere in position without the reflectance sphere. (Note that this is different from $V_{t,\mathrm{ref0}}$ where the sphere is rotated; see Section 3.) The correction factors F_1 to F_4 account for the exchange of light between the spheres through the sample. The noise signals in each sphere may be considered to be diffuse light sources, and therefore the correction factors may be calculated under the assumption that the sample has been illuminated in the reflectance sphere with a relative power $V_{r,\mathrm{ref0}\%}$ and in the transmittance sphere with a relative power of $T_c V_{t,\mathrm{ref0}'\%}$. The T_c factor is included because the unscattered light contributing to the noise in the transmittance sphere will have been attenuated through scattering and absorption by the sample. For the corrections arising from the noise in the reflection sphere we use the equations for the exchange of light between the two spheres and for diffuse irradiance [Eqs. (7) and (8)] divided by the equation that describes the power detected owing to collimated light being incident on the sphere wall [Eq. (1)] so that

$$F_1 = \frac{(1 - b_{2r}R_d)(1 - b_{2t}R_d)}{(1 - b_{2r}R_d)(1 - b_{2t}R_d) - b_{2r}b_{2t}T_d^2}, \tag{29}$$

$$F_3 = \frac{(1 - b_{2r}R_d)}{b_{1r}} \frac{b_{1t}b_{2r}m_r\alpha_t T_d}{(1 - b_{2r}R_d)(1 - b_{2t}R_d) - b_{2r}b_{2t}T_d^2}. \tag{30}$$

The correction factors arising from the noise in the transmittance sphere may be calculated in a similar manner by including the T_c factor and swapping the r's and t's:

$$F_2 = \frac{T_c(1 - b_{2t}R_d)}{b_{1t}} \times \frac{b_{1r}b_{2t}m_t\alpha_r T_d}{(1 - b_{2t}R_d)(1 - b_{2r}R_d) - b_{2t}b_{2r}T_d^2}, \tag{31}$$

$$F_4 = \frac{T_c(1 - b_{2t}R_d)(1 - b_{2r}R_d)}{(1 - b_{2t}R_d)(1 - b_{2r}R_d) - b_{2t}b_{2r}T_d^2}. \tag{32}$$

Note that this correction is normally not significant, as for most samples, and especially with well-collimated sources, $V_r \gg V_{r,0} > V_{r,\mathrm{ref0}}$, $V_{t,\mathrm{ref0}'}$ and $V_t \gg V_{t,0} > V_{r,\mathrm{ref0}}$, $V_{t,\mathrm{ref0}'}$. Only in examples of high attenuation of the light by the sample and relatively poor collimation is it necessary to make this correction.

6. Experimental Validation

To validate the proposed method of measuring optical properties in combination with the inverse adding–doubling algorithm, we attempted to measure the optical properties of tissue phantoms over a wide range of albedos and optical depths. The two phantom materials chosen were Intralipid-10% and Evans Blue.[26,27] These were chosen because their optical properties permit simulation of tissue. Intralipid-10% is forward scattering ($g \approx 0.7$) and at 632.8 nm is a very weakly absorbing liquid (see Table 4 below). Evans Blue (515 mg in 1 L of isotonic phosphate buffer or 515 mg in 1 L of NaCl buffer) is a weakly scattering and highly absorbing liquid at 632.8 nm. Mixtures of these solutions provide samples with a variety of albedos a and optical depths τ. The absorption coefficient and scattering coefficient may be calculated as is described by Eqs. (24) and (25). The anisotropy of the phantom cannot be changed. However, it ($g \approx 0.7$) is similar to the anisotropy of most tissues that we measured with other techniques (where $g \approx 0.7$–0.95).

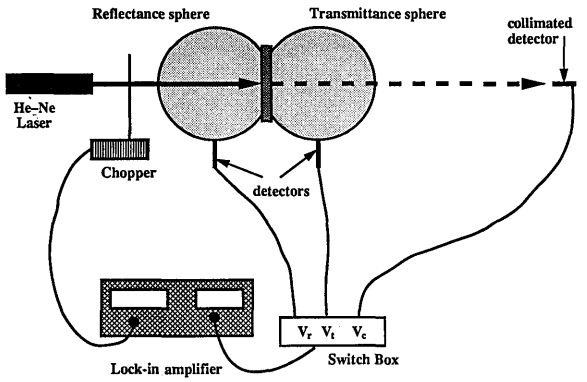

Fig. 3. Experimental apparatus consisting of two integrating spheres with an intervening sample. A He–Ne laser (632.8 nm) directs light directly onto the sample through a chopper. The signal is detected by photodiodes placed on the walls of the two spheres and a distance from the exit port of the transmittance sphere. The signals from the photodiodes and the frequency of the chopper are fed into a lock-in amplifier.

A. Method

A 1-mm 632.8-nm-diameter collimated beam from a 5-m W He–Ne (Uniphase 1105) laser irradiates the sample within the reflectance sphere as shown in Fig. 3. The light within the spheres and the collimated transmission were measured with photodiodes (Telefunken BPW 34) connected to a lock-in amplifier (EG&G Princeton Applied Research 5209). A light chopper was placed in front of the beam for the reference signal to the amplifier. Because of the high level of the collimated signal (without the sample), filters were used with an attenuation factor of $3.73 \pm 0.11 \times 10^{-3}$. We also kept the placement of the collimated diode at a distance (~ 60 cm) from the transmittance sphere as explained in Subsection 5.B to minimize the detection of scattered light. The light was incident at a slight angle to the sample (10.1°), and thus the specularly reflected light is maintained with the spheres. The two spheres were

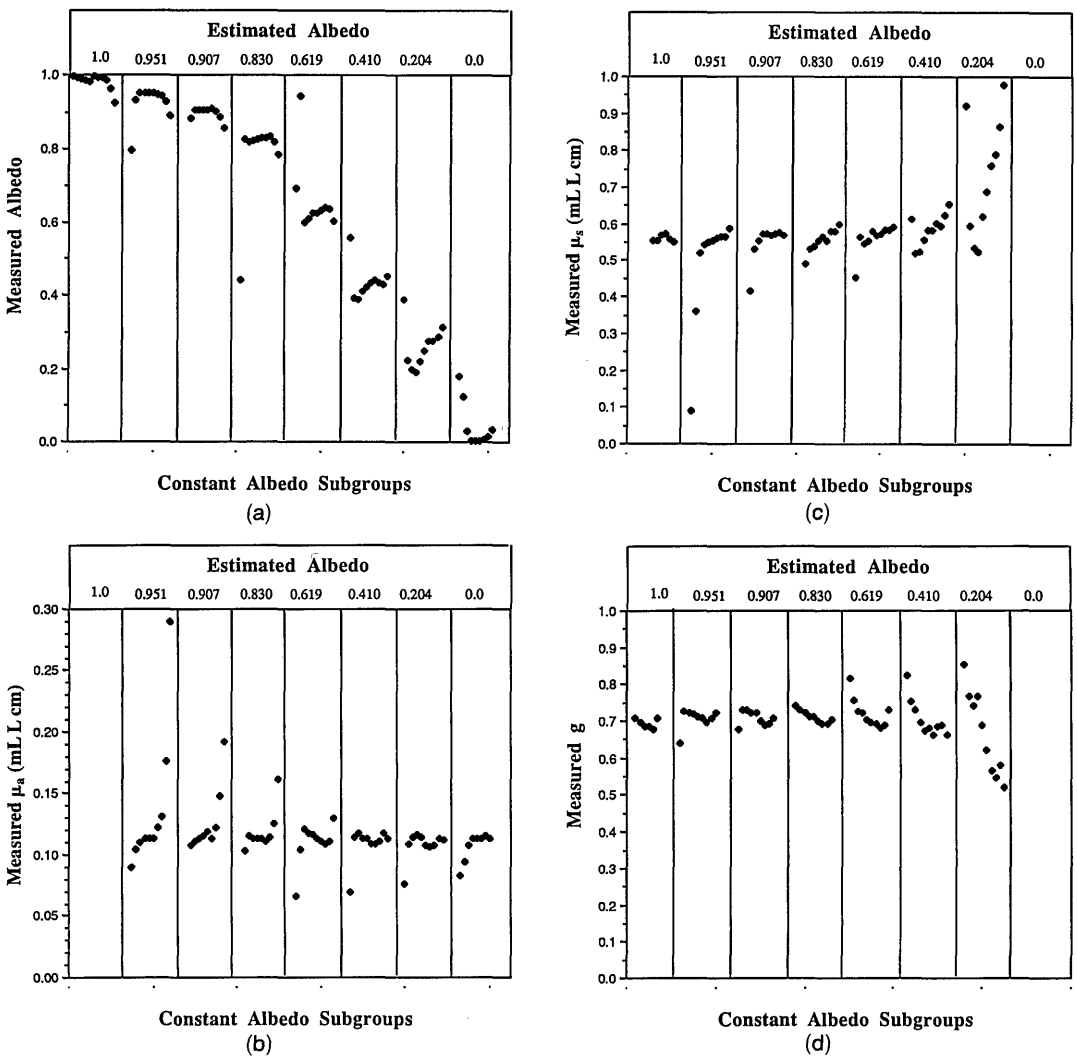

Fig. 4. (a) Measured albedo, (b) anisotropy g, (c) scattering coefficient μ_s, and (d) absorption coefficient μ_a for each subgroup of constant albedo (which is highest at the left and declines to the right). Within each subgroup the optical depth varies from a maximum of 16.3 to a minimum of 0.1. The highest optical depth is always at the left of the subgroup and declines to the right.

Table 3. Accuracy to Which Optical Properties Can Be Determined

Restrictions		Accuracy		
Optical Depth	Albedo	in μ_s (%)	in μ_a (%)	in g (%)
$1 < \tau < 10$	$0.4 < a < 0.95$	<5	<5	<5
$(0.4 < V_{3\%} < 5 \times 10^{-5})$	$a < 0.4$	>5	<5	>5
	$a > 0.95$	<5	>5	<5

geometrically identical with an inner surface area A of 148 ± 1 cm^2, a sample area A_s of 4.90 ± 0.06 cm^2, a detector area A_δ of 0.09 ± 0.02 cm^2, and a total other aperture area of 0.33 ± 0.01 cm^2. The reflectance sphere had a surface reflectance m_r of 0.912 ± 0.005 and the transmittance sphere m_t of 0.915 ± 0.005.

Eighty different phantoms were made in subgroups of fixed albedo (with the same ratio of scatterer to absorber) and varying optical depth (differing dilution). The albedo subgroups were estimated to have albedos of 0, 0.204, 0.410, 0.619, 0.830, 0.907, 0.951, 1.0. At each albedo there were 10 optical depths that varied from 0.1 to 16.3 but were concentrated in the 1–10 range. The thickness of the sample holder was 1.0 mm, and the reference plate was $R_{\text{ref}} = 0.92 \pm 0.02$.

All phantoms of an albedo subgroup maintain the same albedo because the basic solution is just diluted so that a different optical depth is obtained. The inaccuracy within the construction of the phantoms was at most 1% except for the two most diluted phantoms (lowest optical depth) of each subgroup when it was 3%.

B. Results

In Figs. 4(a)–4(d) the subgroup with the highest albedo is always on the left and the albedo decreases to the right. The leftmost subgroup consists of Intralipid-10% only (which is assumed to be scattered only and therefore with an estimated albedo of 1), and the rightmost subgroup is Evans Blue (which is assumed to be absorbing only and therefore with an estimated albedo of 0). Within each subgroup the highest optical depth is the leftmost experiment, and the optical depth decreases to the right.

Figure 4 shows the albedo, anistotropy, scattering coefficient, and absorption coefficient for each experiment. For the majority of points within each subgroup the measured albedo is constant [Figure 4(a)]. Similarly within each subgroup and between each subgroup the measured anisotropy, scattering coefficient (per unit concentration), and absorption coefficient (per unit concentration) are constant as would be expected [Figs. 4(b)–4(d), respectively]. The greatest deviations from the constant values appear to occur when the albedo is very large or very small or within a subgroup when the optical depth is very large or very small.

The average values of the optical properties for all converging data points are as follow:

$$g = 0.70 \pm 0.05,$$

$$\mu_{so} = (0.6 \pm 0.1)\ \text{mL}^{-1}\ \text{L cm}^{-1},$$

$$\mu_{ao} = (0.12 \pm 0.03)\ \text{mL}^{-1}\ \text{L cm}^{-1}.$$

Using pure solutions of Intralipid-10% or of Evans Blue, we may measure the scattering and absorption coefficient by measurement of the collimated light alone. These measurements yield

$$\mu_{so} = (0.56 \pm 0.03)\ \text{mL}^{-1}\ \text{L cm}^{-1},$$

$$\mu_{ao} = (0.115 \pm 0.002)\ \text{mL}^{-1}\ \text{L cm}^{-1}$$

which are in good agreement with the average values determined by the adding–doubling method.

For every data point the relative deviation from the mean may be calculated [deviation = $100\% \times (x - \bar{x})/\bar{x}$]. For each of the optical properties the deviation as $\gtrless 5\%$ is given in Table 3 as a function of the albedo and optical depth. The anisotropy, scattering, and absorption coefficients were all determined with a <5% deviation when the optical depth was between 1 and 10 and the albedo was between 0.4 and 0.95.

Table 4. Optical Properties of Tissue Phantoms

Source	Wavelength (nm)	Intralipid-10% μ_a[a] ($\times 10^{-2}$)	Intralipid-10% μ_a[a] ($\times 10^{-4}$)	Intralipid-10% g	Evans Blue μ_a ($\times 10^{-2}$)
Van Staveren *et al.*[b]	632.8	47.6 ± 0.9	1.49 ± 0.04	0.768 ± 0.006	
Moes *et al.*[c]	632.8	38.6 ± 0.4	5.7 ± 1.5	0.71 ± 0.03	7.60 ± 0.05
Marijnissen and Star[d]	630	55.0		0.83	
This work[e]	632.8	57 ± 13		0.70 ± 0.05	11.5 ± 2.4
This work[f]	632.8	56.1 ± 2.8			11.5 ± 0.2

[a]In units of $\text{mL}^{-1}\ \text{L cm}^{-1}$.
[b]Ref. 27.
[c]Ref. 26.
[d]Ref. 10.
[e]Small spheres, 80 phantoms total.
[f]Collimated transmission measurements only.

The measured optical properties of Intralipid-10% and Evans Blue compare favorably with measurements made with other techniques (Table 4).

7. Discussion

The theory of the integrating sphere allows the description of uncertainties in the reflectance and transmittance measurements of a sample. These uncertainties suggest that collimated incident light is preferential to diffuse incident light. Furthermore, the additional measurement of the transmitted collimated light, together with the inverse adding–doubling algorithm, permits the determination of the three intrinsic properties of the issue, absorption coefficient μ_a, scattering coefficient μ_s, and anistropy factor g.

The double integrating spheres, without significant loss of accuracy, allow the simultaneous measurement of the optical properties, which is a requirement if the tissue is to undergo some external stimulus such as heating.

One should use a large sample diameter compared with the beam diameter to avoid light loss through the side of the sample and by light transport down the glass slide (an ~25-mm aperture for a 1-mm diameter beam). Thus the sample area is large enough that we avoid the light loss problem; yet it is small compared with the surface area of the sphere. (A sample area that is large compared with the surface area of the sphere, >5%, introduces further geometric irregularities not accounted for in the theory of double integrating spheres.[25]

For coherent collimated light the problem of interference caused by the glass slides may be overcome with wedge-shaped slides.

The phantom measurements (Intralipid-10% and Evans Blue) in conjunction with the inverse adding–doubling algorithm enabled the determination of all three optical properties to better than 5% accuracy when the optical depth was between 1 and 10 and the albedo was between 0.4 and 0.95. The inaccuracies at greater optical depths were due to the difficulties in obtaining accurate collimated transmission measurements. This is a limitation in our detecting system rather than in the methodology. The employment of a photomultiplier rather than a photodiode could be expected to improve this measurement. For low albedos and low optical depths the inaccuracy in the results may be due to the uncertainties that arise when the reflectance is low (see Fig. 3 and Section 4). Furthermore, at low optical depths the scattered reflected and transmitted light may not be totally diffuse (Lambertian) as was assumed in the calculations for the integrating spheres.[25] This may lead to a greater loss of light through the entrance port of the reflectance sphere and the exit port of the transmittance sphere than is accounted for.

Finally we recommend this method (in conjunction with the inverse adding–doubling algorithm) for its relative speed of calculation as well as its ability for simultaneous calculation of μ_a, μ_s, and g.

These investigations are in the program of the Foundation for Fundamental Research into Matter and have been supported by The Netherlands Technology Foundation grant VNS88.1426. We gratefully acknowledge the technical assistance of A. Steenbeek and M. Geerts.

References

1. S. A. Prahl, M. J. C. van Gemert, and A. J. Welch, "Determining the optical properties of turbid media using the adding–doubling method," Appl. Opt. **32,** 559–568 (1993).
2. W.-F. Cheong, S. A. Prahl, and A. J. Welch, "A review of the optical properties of biological tissues," IEEE J. Quantum Electron. **26,** 2166–2185 (1990).
3. F. P. Bolin, L. E. Preuss, R. C. Taylor, and R. J. Ference, "Refractive index of some mammalian tissues using a fiber-optic cladding method," Appl. Opt. **28,** 2297–2303 (1989).
4. S. L. Jacques, C. A. Alter, and S. A. Prahl, "Angular dependence of He–Ne laser light scattering by human dermis," Lasers Life Sci. **4,** 309–333 (1987).
5. S. T. Flock, B. C. Wilson, and M. S. Patterson, "Total attenuation coefficients and scattering phase functions of tissues and phantom materials at 633 nm," Med. Phys. **14,** 835–841 (1987).
6. R. Marchesini, A. Bertoni, S. Andreola, E. Melloni, and A. E. Sichirollo, "Extinction and absorption coefficients and scattering phase functions of human tissues *in vitro,*" Appl. Opt. **28,** 2318–2324 (1989).
7. J. R. Zijp and J. J. Ten Bosch, "Angular dependence of HeNe-laser light scattering by bovine and human dentine," Arch. Oral Biol. **36,** 283–289 (1991).
8. L. O. Svassand and R. Ellingsen, "Optical properties of human brain," Photochem. Photobiol. **38,** 293–299 (1983).
9. B. C. Wilson, W. P. Jeeves, and D. M. Lowe, "*In vivo* and postmortem measurements of the attenuation spectra of light in mammalian tissues," Photochem. Photobiol. **42,** 153–162 (1985).
10. J. P. A. Marijnissen and W. M. Star, "Quantitative light dosimetry *in vitro* and *in vivo,*" Lasers Med. Sci. **2,** 235–242 (1987).
11. R. A. J. Groenhuis, J. J. Ten Bosch, and H. A. Ferwerda, "Scattering and absorption of turbid materials determined from reflection measurements. 2: measuring method and calibration," Appl. Opt. **22,** 2463–2467 (1983).
12. J. M. Schmitt, G. X. Zhou, E. C. Walker, and R. T. Wall, "Multilayer model of photon diffusion in skin," J. Opt. Soc. Am. A **7,** 2141–2153 (1990).
13. J. S. Macleod, D. Blanc, and M. J. Cottes, "Measurement of the optical absorption coefficients at 1.06 μm of various tissues using the photoacoustic effect," Lasers Surg. Med. **8,** 143 (A) (1988).
14. U. Bernini, M. Marotta, G. Martino, and P. Russo, "Spectrophotoacoustic method for quantitative estimation of haem protein content in wet tissue," Phys. Med. Biol. **36,** 391–396 (1991).
15. M. S. Patterson, B. Chance, and B. C. Wilson, "Time resolved reflectance and transmittance for the noninvasive measurement of tissue optical properties," Appl. Opt. **28,** 2331–2336 (1989).
16. K. M. Yoo, F. Liu, and R. R. Alfano, "Angle and time resolved studies of backscattering of light from biological tissues," in *Laser–Tissue Interaction,* S. L. Jacques, ed., Proc. Soc. Photo-Opt. Instrum. Eng. **1202,** 260–271 (1990).
17. F. H. Long, N. S. Nishioha, and T. F. Deutsch, "Measurement of the optical and thermal properties of biliary calculi using pulsed photothermal radiometry," Lasers Surg. Med. **7,** 461–466 (1987).
18. S. A. Prahl, I. A. Vitkin, U. Bruggemann, B. C. Wilson, and

R. R. Anderson, "Determination of optical properties of turbid media using pulsed photothermal radiometry," Phys. Med. Biol. **37,** 1203–1218 (1991).
19. A. H. Taylor, "The measurement of diffuse reflection factors and a new absolute reflectometer," J. Opt. Soc. Am. **4,** 9–23 (1920).
20. J. A. Jacquez and H. F. Kuppenheim, "Theory of integrating sphere," J. Opt. Soc. Am. **45,** 460–470 (1954).
21. G. E. Miller and A. J. Sant, "Incomplete integrating sphere," J. Opt. Soc. Am. **48,** 828–831 (1958).
22. D. G. Goebel. "Generalized integrating-sphere theory," Appl. Opt. **6,** 125–128 (1967).
23. F. J. J. Clarke and J. A. Compton, "Correction methods for integrating sphere measurements of hemispherical reflectance," Color Res. Appl. **11,** 253–262 (1986).
24. A. Roos, "Interpretation of integrating sphere signal output for nonideal transmitting samples," Appl. Opt. **30,** 468–474 (1991).
25. J. W. Pickering, C. J. M. Moes, H. J. C. M. Sterenborg, S. A. Prahl, and M. J. C. van Gemert, "Two integrating spheres with an intervening scattering sample," J. Opt. Soc. Am. A **9,** 621–631 (1992).
26. C. J. M. Moes, M. J. C. van Gemert, W. M. Star, J. P. A. Marijnissen, and S. A. Prahl, "Measurement and calculations of the energy and fluence rate in scattering and absorbing phantom at 633 nm," Appl. Opt. **28,** 2292–2296 (1988).
27. H. J. van Staveren, C. J. M. Moes, J. van Marle, S. A. Prahl, and M. J. C. van Gemert, "Light scattering in Intralipid-10% in the wavelength range 400–1100 nm," Appl. Opt. **30,** 4507–4514 (1991)